THE ASTROPHYSICAL JOURNAL, 584:L33–L37, 2003 February 10

THE FIRST SPATIALLY RESOLVED MID-INFRARED SPECTROSCOPY OF β PICTORIS

A. J. WEINBERGER
Department of Terrestrial Magnetism, Carnegie Institution of Washington, 5241 Broad Branch Road, NW, Washington, DC 20015; weinberger@dtm.ciw.edu
AND
E. E. BECKLIN AND B. ZUCKERMAN
Division of Astronomy, University of California at Los Angeles, Box 951562, Los Angeles, CA 90095-1562; becklin@astro.ucla.edu, ben@astro.ucla.edu
Received 2002 September 13; accepted 2002 December 26; published 2003 January 14

ABSTRACT

Long-slit spectra probe the southwest side of the disk in the 8–13 μm region. Dust within 0.″8 of the star shows silicate emission features, including amorphous and crystalline species. Farther out, the disk spectra are featureless and are entirely dominated by dust thermal continuum emission. Mid-infrared imaging of β Pictoris reveals spatial asymmetries in its dusty circumstellar disk at a spatial resolution of 0.″5. Visible for the first time is an inner ($r < 20$ AU) warp in the disk that is aligned differently from a larger scale warp observed in scattered light by the *Hubble Space Telescope*. At 12 μm, as has been observed before, the southwest extension of the disk is brighter than the northeast side. This asymmetry appears to be not as significant at 18 μm. The spatially resolved spectra show that this asymmetry cannot be accounted for by small dust grains that have a spectral feature.

Subject headings: circumstellar matter — radiation mechanisms: thermal — stars: individual (β Pictoris) — techniques: spectroscopic

1. INTRODUCTION

The discovery of excess infrared emission from the nearby star β Pictoris in the *Infrared Astronomical Satellite* (*IRAS*) data (Gillett 1986) resulted in intense study of this A5 IV star. Imaging of the disk in scattered light (Smith & Terrile 1984) and discovery of trace circumstellar gas (Hobbs et al. 1985) quickly suggested the existence of a planetary debris disk. The distance to β Pic is now well established by *Hipparcos* mission astrometry at 19.3 ± 0.2 pc. Its age, 12^{+8}_{-4} Myr, has recently been determined from lower mass members of its comoving group (Barrado y Navascués et al. 1999; Zuckerman et al. 2001). Thus, β Pic is one of the youngest, closest stars to Earth.

Ground-based infrared observations gave the first direct compositional information on the dust when they showed silicate emission similar to that in solar system comets (Telesco & Knacke 1991; Knacke et al. 1993). *Infrared Space Observatory* (*ISO*) spectra, while confirming these features, showed little correspondence between the disk and the comet Hale-Bopp at longer wavelengths (Pantin, Waelkens, & Malfait 1999).

Asymmetries in the disk have been observed in scattered and emitted light at all spatial scales. In scattered light at radii greater than 20″ (400 AU), the northeast (NE) side of the disk is brighter than the southwest (SW) side (Kalas & Jewitt 1995). At radii 40–120 AU, a warp is observed in the disk (Mouillet et al. 1997; Heap et al. 2000). In emitted radiation at 12 μm, the SW side of the disk is brighter (Lagage & Pantin 1994). Large-scale asymmetries in the disk may be explained by the near passage of another star (Kalas et al. 2000), and small-scale asymmetries may be evidence of dynamical perturbations induced by planets within it, just as the zodiacal cloud in our own solar system is sculpted by the planets (Augereau et al. 2001). We have obtained spatially resolved imaging and spectra of the disk of β Pic that clarify the spatial distribution and composition of its dusty material.

2. OBSERVATIONS, DATA ANALYSIS, AND PHOTOMETRY

Mid-infrared observations were taken at the W. M. Keck Observatory on 2000 December 11 with the facility Long Wavelength Spectrograph (LWS; Jones & Puetter 1993). LWS uses a 128 × 128 pixel Boeing Si:As detector and has a plate scale of 0.″08 pixel^{-1}, resulting in a focal plane field of view of 10.″24 square. It also provides a dispersion of 0.037 μm pixel^{-1}; when combined with a 6 pixel (0.″48) slit, the resolution is $R \sim 120$. Vignetting through the long slit limited the field of view to 8.″5. The atmospheric transparency was excellent, with low water vapor optical depth and no clouds. As measured at the Caltech Submillimeter Observatory, the 225 GHz optical depth was ~0.05. Standards measured in both filters at small (1–1.5) air mass throughout the night showed only 6% photometric variation. The air-mass correction was based on the standard star photometry at small air mass and the point spread function (PSF) photometry at large air mass, and it was 5% per air mass at 11.7 μm and 25% per air mass at 17.9 μm, which are reasonable for a dry night at a high-altitude site. Observations were made of β Pic and a nearby PSF reference star, HR 2553, as they transited at an air mass of 3.0 (Table 1). The data were taken in a chop-nod mode with a chopper throw of 5″ north-south at 2 Hz for spectroscopy and 12 μm imaging and 5 Hz for 18 μm imaging. The telescope was nodded 5″ north-south every ~12 s. In imaging mode, this scheme placed an image of the star on the detector in all four chop-nod positions. In each set, the four images were double differenced to produce a final image with one positive and two negative images of the star. Then the star centroid was measured, and all of the differenced images were aligned at the location of the positive star image in the first set. The filters employed had wavelength bandpasses of 11.2–12.2 and 16.9–18.9 μm and are hereafter referred to by their central wavelengths of 11.7 and 17.9 μm, respectively.

The images of β Pic were flux-calibrated based on photometry of the PSF star, HR 2553, from the *IRAS* Faint Source Catalog. The flux densities of the PSF star, after color correction from the catalog values to a slope of ν^2, are 23.5 Jy (0.20 mag) at 12 μm and 5.79 Jy (0.16 mag) at 25 μm. These were also assumed to be the PSF magnitudes in the 11.7 and 17.9 μm LWS filters, respectively. We estimate the uncertainty in this calibration process at 10% in each band, which dominates the statistical (photon counting) uncertainty in the images. The resulting total β Pic

TABLE 1
LOG OF OBSERVATIONS

Mode	Object	Filter Center (μm)	Integration Time (s)	Nods	Air Mass
Imaging	β Pic	11.7	216	8	3.13
	β Pic	11.7	216	8	3.19
	HR 2553	11.7	81	3	3.03
	β Pic	17.9	225	8	3.28
	β Pic	17.9	225	8	3.37
	HR 2553	17.9	56	2	3.00
	HR 2553	17.9	56	2	3.01
Spectroscopy	β Pic	10.3	624	26	3.28
	β Pic	10.3	624	26	3.05
	β Pic	10.3	624	26	3.03
	HR 2553	10.3	72	3	3.07
	HR 2553	10.3	72	3	3.09
	HR 2553	10.3	72	3	3.12

disk plus stellar flux densities are 2.54 ± 0.25 Jy in the 11.7 μm filter and 3.35 ± 0.33 Jy in the 17.9 μm filter. The β Pic photometry agrees well with the published photometry by Backman, Gillett, & Witteborn (1992).

Three two-dimensional spectra, each composed of 26 nod sets, of the SW side of the β Pic disk were taken with the star in the bottom half of the detector. Three two-dimensional spectra, each composed of three nod sets, were taken on the PSF in the same manner. All spectral data were taken in a chop-nod mode, and after double differencing, all of the nod sets were aligned spatially. Nod sets that, due to image wander, were too close to the array edge were eliminated, leaving 66 nod sets in the final β Pic spectrum and nine in the PSF spectrum.

An average one-dimensional spectrum of the PSF star was extracted by fitting a Gaussian at every spectral pixel location. The two-dimensional β Pic spectra were binned in the spatial direction, i.e., along the disk, in 5 pixel wide bins, with the first bin centered on the star. This created 10 one-dimensional spectra at 0.″4 intervals along the disk. Each of these one-dimensional spectra was divided by the average PSF spectrum and then multiplied by the Planck function at the temperature of the PSF star to recover the intrinsic β Pic spectrum at every location. Terrestrial ozone strongly absorbs the stellar continuum around 9.6 μm in a time- and air-mass–dependent way, so it does not calibrate out well. The spectral region from 9.4 to 9.8 μm was therefore excluded from further analysis.

At any given location, the spectrum of the β Pic disk contains a contribution from the disk at that location and from unresolved stellar flux distributed spatially by the effects of diffraction and seeing. Atmospheric seeing dominated the size of the image with a FWHM of 0.″5 (6 pixels) at 11.7 μm. The two-dimensional PSF spectral image was binned in the same manner as the β Pic spectral image discussed above, and the flux contributed from the PSF at every spatial location was measured in each binned spectrum. For every β Pic spectral location, the contribution due to the photosphere was subtracted off, assuming it behaved as a Rayleigh-Jeans function at the star's effective temperature. The photospheric flux density was taken to be 1.177 Jy at 11.7 μm based on an extrapolation of the *L*-band measurement of Backman et al. (1992).

3. RESULTS

3.1. *Imaging*

Images of β Pic at 11.7 and 17.9 μm are shown in Figure 1. The disk can be seen to extend ~4″ (77 AU) from the star. These

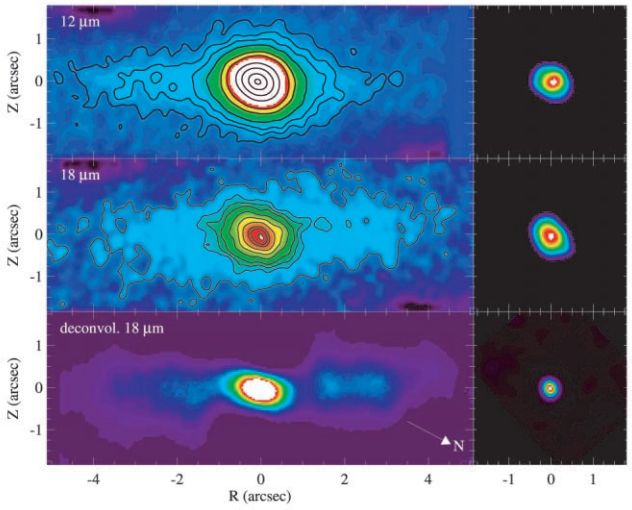

FIG. 1.—*Top*: Image of the star plus disk of β Pic at 11.7 μm (*left*) with contours drawn at 1 (=7.3 mJy arcsec^{-2}), 3, 4, 5, 7, 8, 11, 13, 14, and 15 σ and a corresponding 11 μm PSF (*right*). *Middle*: Image at 17.9 μm (*left*) with contours drawn at 1 (=21.4 mJy arcsec^{-2}), 2, 3, 5, 10, 15, 30, 45, 65, and 80 σ and a corresponding 17.9 μm PSF (*right*). *Bottom*: 17.9 μm image after 13 iterations of Lucy-Richardson deconvolution (*left*) and a similarly deconvolved 17.9 μm PSF image (*right*). The peaks and warps in the disk at radii of ~2″ in the deconvolved image have signal-to-noise ratios of only 1–3 per resolution element. However, a tilt in the inner 1″ disk is evident even in the raw image at 18 μm. In all images, north is 124° from vertical (+*Z*), as shown by the arrow in the bottom plot.

images are seeing-limited at a resolution of ~0.″5. The central region of the disk (saturated on this color stretch) is also extended compared with the PSF. The SW side of the disk is brighter and more extended at 12 μm but approximately equal in surface brightness to the NE side at 18 μm, consistent with previous results of Pantin, Lagage, & Artymowicz (1997) at a slightly poorer spatial resolution. There is no evidence of a point source other than the star.

The disk images were fitted with elliptical isophotes to determine the position angles reported in Table 2. At radii of 1″–4″, our results agree to within the uncertainties with the angles measured in scattered light by Heap et al. (2000) and Mouillet et al. (1997) over the same region. Because it is oriented 4.°6 east of the large-scale scattered light disk, those authors refer to this region as the "inner warp." At a radius of 1.″0, there appears to be an abrupt discontinuity between this previously imaged region and a central portion of the disk visible for the first time in mid-infrared images. Within a radius of 1″, the mid-infrared images clearly show a portion of the disk that is tilted 16° west of the previously imaged 1″–4″ portion. The tilt is a consistent feature in all the nod sets obtained. The tilt geometry is most easily seen in the 18 μm images, in which the contamination of the image by the central star is less. The ellipticity and position angle (P.A.) of this region are constant as a function of radius at 0.27 ± 0.02 and

TABLE 2
DISK POSITION ANGLES

Radius (arcsec)	P.A. (deg)	Reference
0–1	18.5 ± 2.4	This Letter
1–4	33.3 ± 2.0	This Letter
1–5	35.4	Heap et al. 2000
5–20	30.8 ± 0.6	Kalas & Jewitt 1995

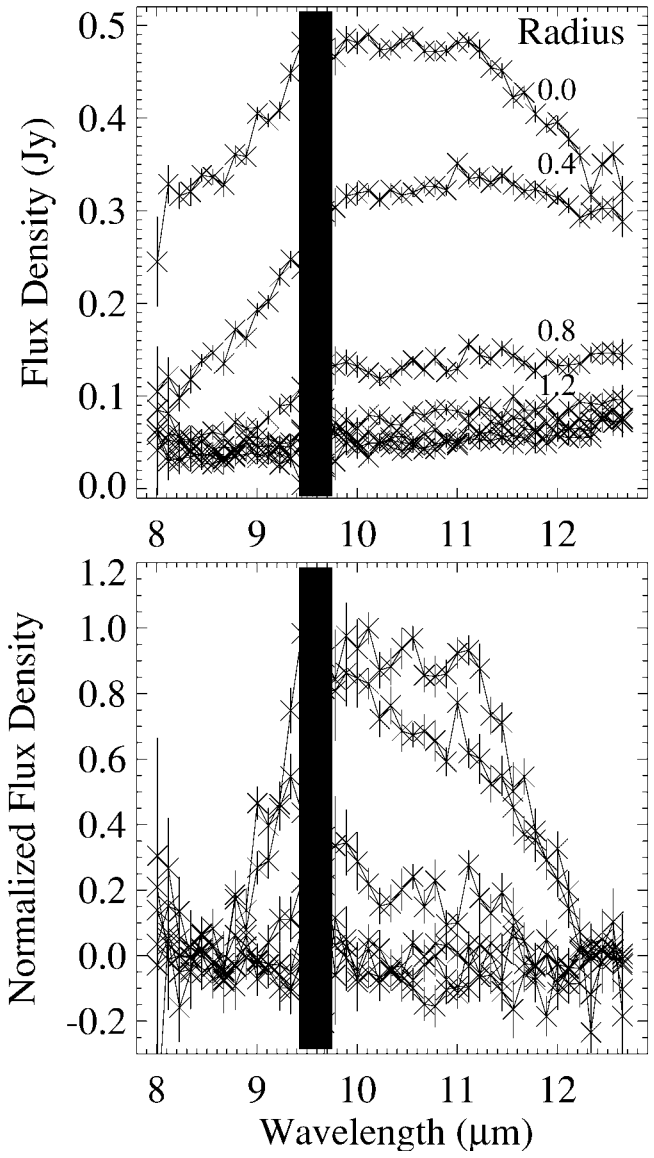

FIG. 2.—*Top*: Spectra of the SW side of the disk (after subtraction of the contribution of the photosphere) shown as a function of radius (the curves shown are, from the top down, binned in 0.″4 intervals centered at radii of 0.″0, 0.″4, 0.″8, 1.″2, 1.″6, 2.″0, and 2.″4). *Bottom*: Spectra after subtraction of a continuum fit to the 12.6 μm/8.2 μm color temperature. Silicates are seen in the first three spectra, but only the continuum is seen at larger radii. The vertical black bar blocks the noisy region contaminated by strong telluric ozone absorption.

18.°5 ± 2.°4, respectively. The shape of the PSF does not have this same behavior. Over the same 0.″6–1″ region, the PSF ellipticity is monotonically decreasing to 0.18 at 1″, and its P.A. is variable with an average of $-14° \pm 5°$.

To better characterize the warp of the disk, a Lucy-Richardson deconvolution of the 18 μm data was performed using one of the PSF observations taken just after the β Pic data. This PSF was also used to deconvolve a second PSF observation (see Fig. 1). The deconvolution algorithm is that in the STSDAS package of IRAF (Snyder 1991) and includes the effect of additive read noise of the detector. The algorithm was allowed to iterate 13 times. The P.A. of the disk within 1″ in the deconvolved image, 21.°1, agrees (1.2 σ) with that measured in the undeconvolved image. The deconvolution also reveals structure in the outer part of the disk, but the signal-to-noise ratios of these variations from a smooth disk are low.

TABLE 3
DISK COLOR TEMPERATURE[a]

RADIUS (AU)	TEMPERATURE		
	Measured (K)	Blackbody (K)	Silicate (K)
"0"	474 ± 16	...	...
7.7	277 ± 9	163	208
15.4	259 ± 11	115	159
23.2	311 ± 19	94	142
30.9	324 ± 26	82	123
38.6	283 ± 20	73	114
46.3	270 ± 17	67	106

[a] As a function of distance from the star along the SW arm as measured in the spectra compared with model blackbody and smoothed astronomical silicate (Drain & Lee 1984) grain temperatures.

3.2. *Spectroscopy*

Shown in the top panel of Figure 2 are 8–13 μm spectra of the SW (brighter) side of the β Pic disk after subtraction of the photospheric component. The spectrum extracted from within 0.″2 of the star agrees very well with that observed previously by Knacke et al. (1993), including a flat-topped profile characteristic of a mixture of amorphous and crystalline silicates.

The temperature of the grains at each radius was estimated by the color temperature measured out of the silicate feature, i.e., at 8.0-8.4 and 12.5–12.7μm, extending as low and as high in wavelength as there were data available. These are given in Table 3. A Planck function at that color temperature was then normalized to the long-wavelength flux and subtracted from each spectrum. The results are shown in Figure 2 (*bottom panel*). At radii less than 1″, a clear contribution from silicates is present, and for these three spectra, the silicate–to–continuum flux ratios and silicate line shapes are equal to within the uncertainties. This implies that the relative abundances of amorphous and crystalline grains remain approximately constant with radius. At radii greater than 1″, flux from the disk is detected in the spectra (see the top panel of Fig. 2). If the silicate–to–continuum flux ratio at these radii were the same as the ratio within 1″, silicate emission would have been detected between 1.″2 and 2.″4.

4. DISCUSSION

The main puzzles to be explained are the various tilts of the disk and its brightness asymmetries in light of the spectroscopic data. The P.A. of the disk does not change monotonically with increasing radius but rather appears to shift discontinuously and in opposite directions at 1″ and ~4″. The discovery of a previously unseen warp in the innermost part of the disk along with the already known warp at 1″–4″ suggests active perturbation of the disk (cf. Wahhaj et al. 2003). The outer warp alone has been modeled as induced by the presence of a giant planet (Augereau et al. 2001). Two planets in orbits inclined to each other could in principle reproduce both warps as well as perhaps explain why the planets' orbits are inclined to the dust disk at all. However, grains must be fairly small to emit efficiently into the 10 μm silicate feature, so our spectra show that within 20 AU, there must be grains of size $\lesssim$10 μm. Such grains are the most susceptible to radiation pressure blowout on an orbital timescale. It remains to be modeled how the grains can be sculpted into warps during their short lifetimes in the disk.

Our spectra also show that the strength of the silicate feature does not decrease with distance until a radius of ~20 AU. In

their model of the grains in this disk, Li & Greenberg (1998) predict that the silicate emission feature comes from grains within 40 AU, and our data are broadly consistent with their model in which grains sublimated from comets produce the mid-infrared emission. However, the grains in comet comae in our own solar system show the same 10 μm band silicate feature seen in β Pic at a wide range of heliocentric distances corresponding to blackbody and observed continuum temperatures of 270–600 K (Hanner, Lynch, & Russell 1994). Cometary silicate–to–continuum flux ratios do not appear to change substantially over this temperature range. Based on the comet data, we would expect to see silicates at all the continuum temperatures measured from our spectra and given in Table 3. The disappearance of the silicate feature beyond 20 AU shown in the bottom panel of Figure 2 therefore indicates a decrease in the ratio of the number of small silicate grains to large grains contributing to the thermal emission at increasing radius from the star.

A higher density of small silicate grains in the inner part of the disk could be due to increased production in close to the star and then the dispersal of the grains to larger radii by radiation pressure, if the outer part of the disk has a parent distribution of larger grains. We do not see a measurable change in the amorphous/crystalline silicate ratio with distance. If grains are being annealed in the inner regions of the disk, then radiation pressure must be transporting them to outer regions efficiently.

The asymmetry of the mid-infrared disk, i.e., that the SW side is brighter than the NE side at 12 μm, could in principle be explained by surface density, composition, or temperature changes within the disk. The disk is optically thin at all wavelengths, so an increase in brightness could be due to an increase in the surface density of emitting grains. If this were the case, as has been noted before by Pantin et al. (1997) and Augereau et al. (2001), the grains would have to be efficient emitters *only* at 12 μm and poor scatterers because otherwise we would expect to see the same level of brightness asymmetry at 18 μm and in the visual scattered light. We would have expected these presumably small, iceless grains at 20–40 AU to show the silicate feature, but our spectra indicate that they do not.

An enhancement in the broadband 12 μm flux density on the SW side could be due to composition if it consisted of material emitting in a spectral feature in that band. However, at the location of the enhanced SW flux, at radii $\sim$2″ from the star, the spectra in Figure 2 show a slowly rising featureless continuum with no emission lines. Therefore, the asymmetry is unlikely to be due to compositional effects.

An increase in temperature on the SW side of the disk could increase the 12 μm flux substantially more than the 18 μm flux. The slowly rising continuum seen in our spectra is consistent with the idea that large grains in the disk are heated primarily by the central star, so they get colder, and emit more at longer wavelengths, at larger distances. However, as seen in Table 3, the temperatures determined from the spectra are substantially hotter than those expected from blackbody grains in thermal equilibrium with the 6.9 $L_{\odot}$ (I. Song 2002, private communication) star. Nor do 0.1 μm "smoothed UV astronomical silicates" (Draine & Lee 1984), which, thanks to their emission properties, reach higher temperatures, reproduce the measured temperatures. A specialized size distribution of very small dust grains could probably explain the high color temperature but would also be expected to show the silicate emission feature. If these grains, despite their susceptibility to radiation pressure blowout, could be captured into a resonance with a planet, then they could also explain the NE/SW dust asymmetry.

The simple heating of dust grains by a small body within the disk is insufficient to produce these temperatures. For example, a 1 $M_{\rm Jup}$ planet at an age of 12 Myr has a luminosity of $\sim 10^{-6}$ $L_{\odot}$ (Burrows et al. 1997). At a distance of 0.1 AU, the dust is heated only an additional 30 K by such a planet. The heating mechanism, if that is indeed the explanation for the enhanced color temperature, remains unknown.

5. CONCLUSIONS

The structure of the β Pic disk can be probed closer to the star, 10–20 AU, with mid-infrared imaging than with scattered-light imaging, even with the *Hubble Space Telescope*. A tilt of the inner disk is revealed in the mid-infrared that, relative to the P.A. of the extended disk beyond 100 AU, is much greater than and in a direction opposite to that of the warp previously observed in scattered light between 20 and 80 AU from the star. The first spatially resolved spectroscopy of the disk shows amorphous and crystalline silicates out to 20 AU from the star. Beyond 20 AU, the proportion of small silicates relative to larger grains decreases. Small grains may be preferentially generated in the inner portion of the disk, because of a higher collisional rate of planetesimals, and then distributed to larger radii by radiation pressure. Spatial asymmetries in the 12 and 18 μm emission cannot easily be explained by compositional or density differences in the disk; they remain mysterious.

This Letter is based on observations at the W. M. Keck Observatory, which is operated as a scientific partnership among the California Institute of Technology, the University of California, and the National Aeronautics and Space Administration, and was made possible by the generous financial support of the W. M. Keck Foundation. We acknowledge support from the UCLA and CIW nodes of the NASA Astrobiology Institute, a NASA Origins grant to UCLA, and the NASA SOFIA project.

REFERENCES

Augereau, J. C., Nelson, R. P., Lagrange, A. M., Papaloizou, J. C. B., & Mouillet, D. 2001, A&A, 370, 447
Backman, D. E., Gillett, F. C., & Witteborn, F. C. 1992, ApJ, 385, 670
Barrado y Navascués, D., Stauffer, J. R., Song, I., & Caillault, J.-P. 1999, ApJ, 520, L123
Burrows, A., et al. 1997, ApJ, 491, 856
Draine, B. T., & Lee, H. M. 1984, ApJ, 285, 89
Gillett, F. C. 1986, in Light on Dark Matter, ed. F. P. Israel (Dordrecht: Reidel), 61
Hanner, M. S., Lynch, D. K., & Russell, R. W. 1994, ApJ, 425, 274
Heap, S. R., Lindler, D. J., Lanz, T. M., Cornett, R. H., Hubeny, I., Maran, S. P., & Woodgate, B. 2000, ApJ, 539, 435
Hobbs, L. M., Vidal-Madjar, A., Ferlet, R., Albsert, C. E., & Gry, C. 1985, ApJ, 293, L29
Jones, B., & Puetter, R. 1993, Proc. SPIE, 1946, 610
Kalas, P., & Jewitt, D. 1995, AJ, 110, 794
Kalas, P., Larwood, J., Smith, B. A., & Schultz, A. 2000, ApJ, 530, L133
Knacke, R. F., Fajardo-Acosta, S. B., Telesco, C. M., Hackwell, J. A., Lynch, D. K., & Russell, R. W. 1993, ApJ, 418, 440
Lagage, P. O., & Pantin, E. 1994, Nature, 369, 628
Li, A., & Greenberg, J. M. 1998, A&A, 331, 291
Mouillet, D., Larwood, J. D., Papaloizou, J. C. B., & Lagrange, A. M. 1997, MNRAS, 292, 896
Pantin, E., Lagage, P. O., & Artymowicz, P. 1997, A&A, 327, 1123

Pantin, E., Waelkens, C., & Malfait, K. 1999, in The Universe as Seen by *ISO*, ed. P. Cox & M.F. Kessler (ESA SP-427; Noordwijk: ESA/ESTEC), 385
Smith, B. A., & Terrile, R. J. 1984, Science, 226, 1421
Snyder, D. L. 1991, in The Restoration of *HST* Images and Spectra, ed. R. L White & R. J. Allen (Baltimore: STScI), 56
Telesco, C. M., & Knacke, R. F. 1991, ApJ, 372, L29
Wahhaj, Z., Koerner, D. W., Ressler, M. E., Werner, M. W., Backman, D. E., & Sargent, A. I. 2003, ApJ, 584, L27
Zuckerman, B., Song, I., Bessell, M. S., & Webb, R. A. 2001, ApJ, 562, L87